

## Residual-state creep of clastic soil in a reactivated slow-moving landslide in the Three Gorges Reservoir Region, China

**Abstract** We study the creep properties of clastic soil in residual state. The intact samples are taken from a reactivated slow-moving landslide in the Three Gorges Reservoir Region, China. Firstly, the patterns of the landslide movement are analysed based on recent monitoring data, which indicate that the soil within the shear zone is undergoing two deformation processes: a creep phase, characterised by different creep rates, and a dormant phase. We then study the creep behaviour of the soil samples through a series of ring shear creep tests under various shear stress conditions. The creep response depends strongly on the ratio of the shear stress to the residual strength, and the normal effective stress, whereas the creep rate decreases due to strength regain. The long-term strength of the clastic soil is close to the residual strength. Therefore, the residual strength obtained from conventional shear test, which is less time consuming than creep test, can be used in long-term stability analyses of creeping landslides.

**Keywords** Clastic soil · Long-term strength · Reactivated landslide · Ring shear · Residual shear strength state

### Introduction

Landslides account for a significant proportion of the geohazards that occur in the Three Gorges Reservoir Region (TGR) of China, potentially causing severe damage to both buildings and city infrastructure (Cascini et al. 2009; Du et al. 2013; Li et al. 2010; Zhou et al. 2014). Most slow-moving landslides deform gradually through phases of episodic acceleration and deceleration corresponding to seasonal rainfall, water level fluctuations at the toe of the slope, and/or changes in material properties within the shear zone (Zangerl et al. 2010). These characteristics make slow-moving landslides difficult to detect, and as a result, constructing new roads, buildings, and tourist resorts in areas prone to slow-moving landslides is risky.

Most reactivated slow-moving landslides in the TGR are characterised by slip surfaces that are generated by shear displacement (Picarelli 2007). The total shear displacement of slow-moving landslides may consist of a plastic shear displacement and a creep component (Mansour et al. 2011; Van Asch 1984). While the creep component is linked to changes in the hydrological boundary conditions, such as the rate of rainfall (Matsuura et al. 2008) and groundwater flow (Cascini et al. 2010; González et al. 2008; Van Asch and Malet 2011; Wang et al. 2008c), it is predominantly governed by the creep properties of the soil in the shear zone. Since the shear zone soil in a reactivated slow-moving landslide has already reached a residual state, any subsequent creeping movement is governed by the drained residual strength (Skempton 1985; Stark et al. 2005; Stark and Hussain 2010b, 2012). This fact can be evidenced by comparing theoretical and actual landslide creep profiles using a model proposed by (Yen 1969). By using the residual strength for shear creep, this model provided

the best prediction of creep velocity validated by field measurements (Van Asch 1984). Therefore, in a creep analysis, it is necessary to investigate the creep properties of the shear zone soil under residual strength conditions. Landslide movement in the TGR, however, is usually characterised by alternating creep and dormant phases (Miao et al. 2014), which correspond to accelerating and decelerating periods of creep, respectively (Wang et al. 2008b). During the creep phase, the weight of the slope overburden is the fundamental driving force of landslide movement. In the dormant phase, shear strength regain may occur in the soil; often, the magnitude of the regained strength is time-dependent (Stark and Hussain 2010a; Bhat et al. 2013a). However, the influence of the periodic dormant phases on the creep behaviour of the landslide shear surface remains unclear.

Many laboratory tests have been conducted to investigate the creep properties of soils within the shear zone, using both direct shear and triaxial testing apparatuses (Lai et al. 2012; Wang et al. 2008a; Zou and Wang 2010). In most cases, however, researchers have concentrated on pre-failure creep in materials which had not reached residual state. Therefore, these types of experiments may not accurately simulate the stress history within pre-existing landslide shear zones. Recently, several residual-state creep tests, including the reversal direct shear test (Maio et al. 2013; Wen and Jiang 2017) and ring shear test (Bhat et al. 2011, 2013a), have been reported. In these tests, the soil samples were first sheared to residual conditions and then subjected to sustained shear stresses. These studies showed that the reversal direct shear test was not able to achieve a residual state, while the ring shear test was conducted on clayey soils, which are not representative of the typical clastic soil present in reactivated slow-moving landslides in the TGR.

In this paper, we will investigate the effect of the shear stress ratio (the ratio of the applied constant shear stress to the residual strength) on the basic creep properties of the clastic soil during the landslide creep phase and study the influence of strength regain on the creep behaviour during the landslide dormant phase. To do so, we first examine the movement patterns of a slow-moving landslide in the TGR. We then performed a set of ring shear creep tests to simulate the shear process of the clastic soil within the shear zone. Finally, the creep threshold values and the long-term strength of the clastic soil are discussed.

### Patterns of movement in the Huangtupo landslide

The Huangtupo landslide lies on a hill-slope facing the Yangtze River valley, 10 km east of Badong County, as shown in Fig. 1. The geological formations from which this landslide developed are known locally as the Badong Formation ( $T_2b^2$  and  $T_2b^3$ ). The landslide mainly consists of irregular alternations of mudstone, pelitic siltstone, argillaceous limestone, and limestone (Deng et al. 2000; Tang et al. 2015a; Wang et al. 2014). The crown of the

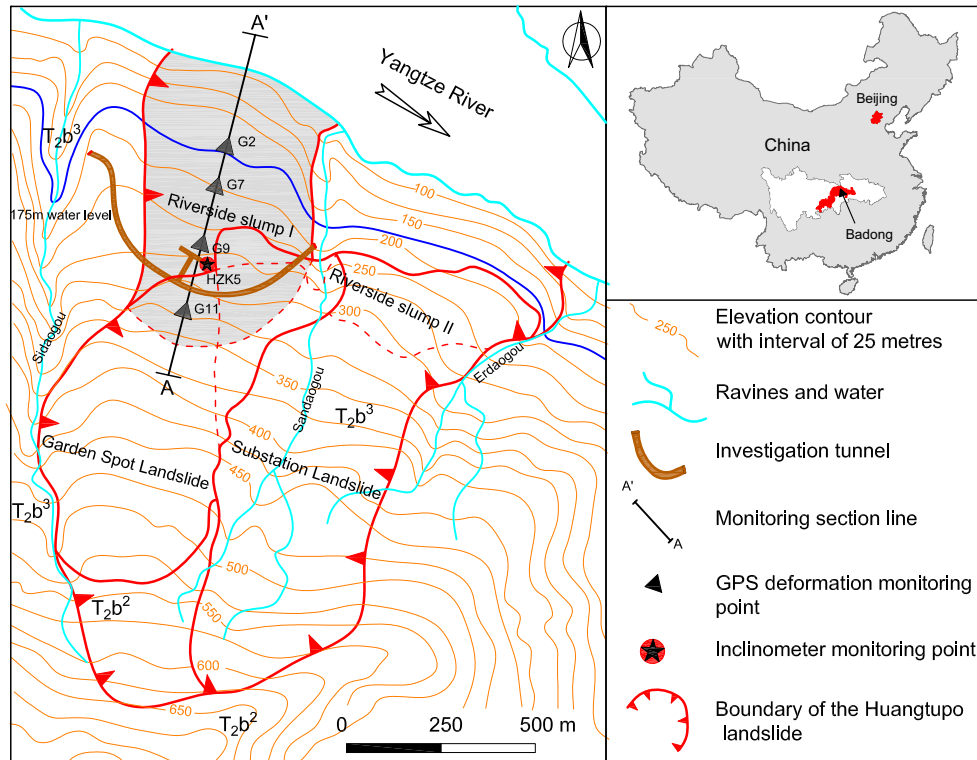


**Fig. 1** Location and plan view of the Badong and Huangtupo landslides (modified after (Wang et al. 2016))

landslide is located at approximately 600 m.a.s.l., while the toe ranges from 50 to 90 m.a.s.l. The toe is submerged in the Yangtze River with water levels varying from 145 to 175 m as regulated by the Three Gorges Dam. The landslide covers a total area of 1,358,104 m<sup>2</sup> and has a volume of nearly 69,107 m<sup>3</sup>; therefore, it is the largest reservoir landslide in the TGR.

The Huangtupo landslide is a complex mass formed by multiple slumps that occurred over a period of at least 40,000 years (Tang et al. 2015b). On the surface, the landslide is divided by the Sandaogou Valley into two groups of sliding masses. Each group is composed of two sliding masses, one above the other, with additional recent sliding masses developing adjacent to the edges of the landslide. The lower slope sliding masses, Riverside Slump I and Riverside Slump II, are adjacent to the Yangtze River; their toes are submerged in the river, and their crowns are overlain by the younger Garden Spot Landslide and Substation Landslide, respectively. The Riverside slumps are chaotic slump masses consisting of either loose or dense soil and rock debris that originated from grey pelitic limestone and grey limestone (Wang et al. 2014). Figure 2 shows the geological profile of Riverside Slump I.

Previous studies conducted on the Huangtupo landslide, focus on subjects such as its soil properties (Jiao et al. 2014; Wang et al. 2012), stability (Cojean and Cai 2011), formation mechanisms (Deng et al. 2000), triggering factors (Wang et al. 2014), and kinematic features (Tang et al. 2015b; Tomás et al. 2014). Despite these detailed investigations, landslide movement under various hydraulic boundary conditions represents one of the most pressing concerns for slope failure prevention and control. Based on three sets of radar data, Tomás et al. (2014) reported that the upper part of the slope is affected by seasonal displacements caused by

rainfall, while the lower part of the slope is affected by water fluctuations in the Yangtze River. Furthermore, whereas Riverside Slump I exhibits predominantly downward movements that range from very slow (17.2 mm/year) to extremely slow (12.8 mm/year), the other landslides are relatively stable. The definition for describing the rate of movement of a landslide can be found in literature (IGUS/WGL 1995; Mansour et al. 2011).

Recently, the first comprehensive 3-D field-testing site has been constructed, including investigation tunnels beneath the landslide and monitoring systems on the slope surface (see Fig. 2), enabling the study of the kinematic features of the Huangtupo landslide (Tang et al. 2015b; Wang et al. 2014). In situ GPS monitoring has indicated that Riverside Slump I is steadily creeping, with a maximum deformation direction towards 20° northeast and a rate of approximately 15 mm/year (Tang et al. 2015b), as shown in Fig. 3a. This slow creep rate had previously allowed the landslide to deform undetected within the area chosen for the site of old Badong. In the years following the construction of old Badong, landslide movements caused damage to both buildings and infrastructure, and the number of seriously damaged houses steadily increased.

Two major shear zones, characterised by yellow and light-grey clay with small gravel clasts and slickensides, were exposed during the excavation of the investigation tunnels. At that time, it was noted that a large displacement had occurred in the shear zone, associated with either a previous landslide or tectonic shearing. Evidence found since indicates that these represent landslide shear zones of the reactivated slow-moving landslide has reached a residual state. This evidence includes slickensides commonly observed in the matrix materials supporting the gravel clasts, as well

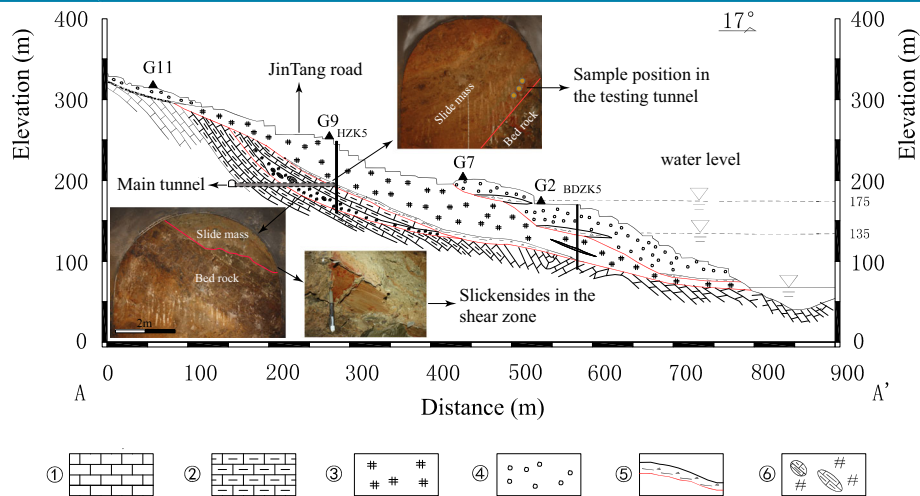


**Fig. 2** Section A-A' in Riverside slump I: ①, limestone; ②, pelitic limestone; ③, dense soil and rock debris; ④, loose soil and rock debris; ⑤, shear zones with possible slip surfaces; ⑥, Mudstone fraction zone

as microscopic platy clay minerals observed in the shear zones and on the slipping surface (see Fig. 2). Inclinator monitoring, the results of which are shown in Fig. 3b, has revealed that the landslide shear zone localise most of the creep displacement, with the upper shear zone experiencing greater net creep displacement than that of the lower shear zone.

The upper shear zone has undergone a significant amount of creep displacement since the investigation, causing several cracks to form in the pavement of the investigation tunnel. Therefore, extensometers were installed to measure the propagation of these cracks since August 2013. Figure 4 presents the development of a 2-cm crack near the shear zone from August 2013 to December 2014, to some extent providing an insight into the patterns of movement in the Huangtupo landslide. The creep displacement increases stepwise, the differentiation of which yields several stages of varying displacement rates with either increasing or decreasing trends. The development of this crack is certainly related to the

intermittent phases of landslide acceleration and deceleration in the apparent dip direction of the shear plane. Therefore, the landslide has experienced alternating accelerating and decelerating movements, denoting the creep phases and dormant phases, respectively. More information concerning the development of all the cracks in the investigation tunnel pavement can be found in the literature (Wang et al. 2016).

Variation in the groundwater table is considered a significant factor influencing the movement of slow-moving landslides (Cascini et al. 2010; Corominas et al. 2005; Leung and Ng 2013; Prokešová et al. 2012). Figure 5 presents crack displacement in relation to water level fluctuations in the TGR and rainfall records in Badong district. The shaded sections of the figure show the creep processes coincide with the periods of intensive rainfall and significant declines in TGR water level. However, there is a delayed response to seasonal rainfall and decreasing water level because the changes in pore water pressure in the shear zone depend on the hydraulic conductivity, and thickness of the sliding mass, as well as the externally applied load (Miao et al. 2014). Although displacement is affected by hydraulic boundary conditions, the creeping movement continues to increase. The main conclusion drawn from this analysis is that the creeping movement of the Huangtupo landslide is predominantly governed by its self-weight. Affected by some external factors, the soil within the shear zone is undergoing two deformation processes: the creep phase at different creep rates and the dormant phase with different periods.

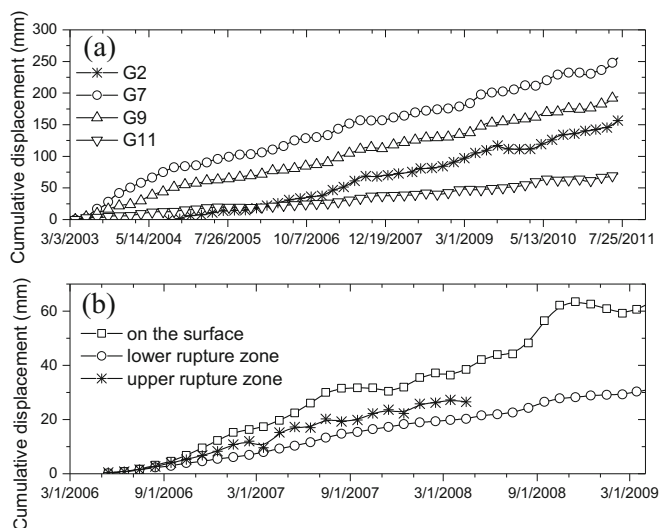


**Fig. 3** Monitoring results. a Cumulative displacement of Riverside slump I, based on data from (Wang et al. 2014). b Creep displacement on the surface and in the upper and lower rupture zones, obtained from inclinometer HZK5

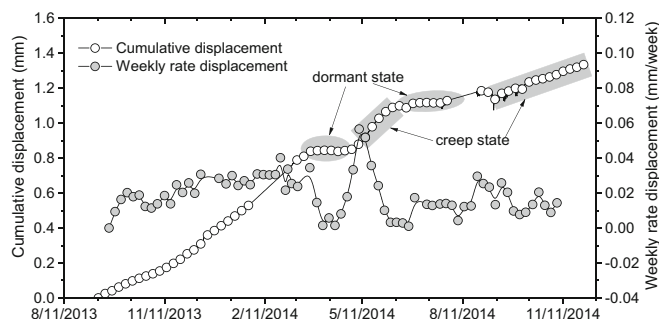


**Fig. 4** Crack development curve and weekly rate of displacement

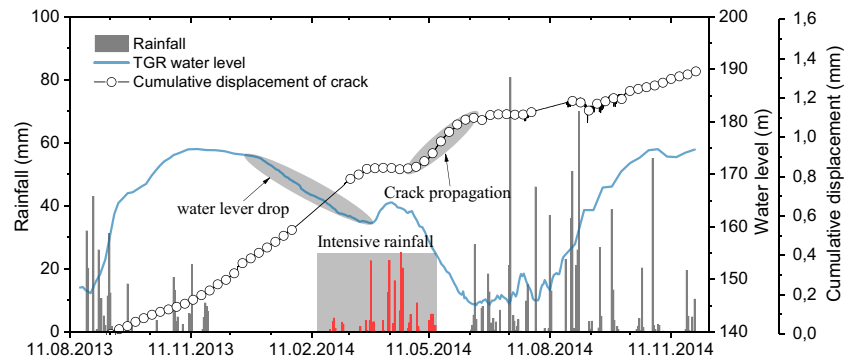


Fig. 5 Effect of TGR water level and Badong District rainfall on crack development in the investigation tunnel

### Ring shear creep tests

#### Test material

The tunnel excavation exposed two main landslide shear zones consisting of three lithologies, namely brown-yellow gravel soil in the slide mass, yellow and light-grey clay with gravel along the shear zone, and bluish-brown and brownish-yellow argillaceous limestone formed in the subjacent stable bedrock (Tang et al. 2015a). Intact samples were collected from the upper shear zone (see Fig. 2); two of these samples (samples HTP1 and HTP2, representing the upper and lower parts of the shear zone, respectively) were analysed to determine their basic properties and grain size distributions.

As presented in Fig. 6a, the shear zone soil typically comprises fine-grained soil (silt + clay) with a significant fraction of coarse-grained particles. Specifically, the finer fraction accounts for between 40.2 and 62.2 wt.% of the total material. The gravel clasts are generally well rounded with diameters varying from 0.5 to 2.5 cm, constituting approximately 20 to 30 wt.% of the material. According to the Casagrande chart shown in Fig. 6b, the examined samples can be classified as silt-clay with low to medium plasticity (HTP1) and silt-clay mixtures of low plasticity (HTP2). The sample physical properties, including indices of the dry density, liquid limit, plastic limit, and plasticity, are listed in Table 1. The soil from the upper part of the shear zone contains higher proportions of clay-like particles. This implies that soil sample HTP1 has a higher creep potential than HTP2 sample. It is desirable to obtain more pronounced viscous behaviour in the creep test; thus, soil sample HTP1 has been used throughout our creep tests.

#### Test apparatus

The ring shear apparatus was originally designed to study the residual strength of soil, but has often been used in the investigation of landslide mechanisms (Okada et al. 2004) and the formulation of shear zones using reconstituted samples (Mandl et al. 1977; Torabi et al. 2007; Jiang et al. 2017). The ring shear apparatus used in the present study was based on a concept proposed by Bishop et al. (1971).

The sample container has a height of 30 mm; the inner and outer rings have diameters of 100 and 150 mm, respectively, resulting in an effective shear area of 98.17 cm<sup>2</sup>. The sample is contained in the shear box confined by the upper and lower ring, with a flexible gap between the upper and lower parts of the shear box. During shearing, the upper ring is fixed, and the lower ring rotates clockwise along a horizontal plane. A total of 12 knives (or ribs) are evenly placed on both the upper and lower porous ring plates to ensure the transfer of torque to the sample. Two transducers below the shearing box measure the shear resistance, and a servo-actuated loading cell controls the normal force, as shown in Fig. 7. This apparatus can simulate different loading conditions while the sample is sheared using either a torque-controlled or shear rate-controlled method. During shearing, the pore water pressure on the surface of the samples, shear strain rate, normal stress, shear strain, axial strain, and environmental temperatures are measured by a data acquisition system.

#### Test programme

Three types of creep curves were simulated in the residual-state creep tests, as schematically shown in Fig. 8. In Fig. 8, line 1

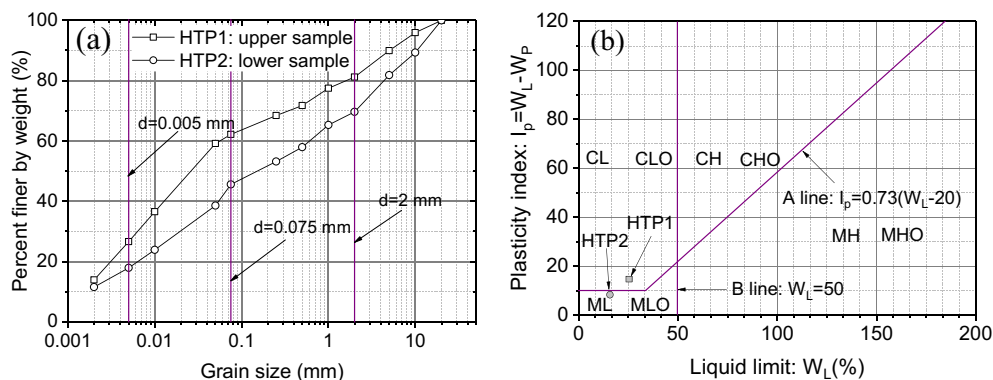


Fig. 6 Indices of physical properties of soil sample from Huangtupo landslide. a grain size distribution. b plasticity

**Table 1** Basic properties of shear zone soil

Sample name	$\rho(\text{g/cm}^3)$	$W(\%)$	$W_L(\%)$	$W_p(\%)$	$I_p(\%)$
HTP1	2.30	17.2	29.1	13.7	15.4
HTP2	2.49	15.3	21.5	12.3	9.2

$\rho$  bulk density,  $W$  water content,  $W_L$  liquid limit,  $W_p$  plastic limit,  $I_p$  plasticity index

characterises the development of creep at a constant strain rate, representing viscous flow; line 3 corresponds to attenuating creep at a decreasing strain rate; and line 2 represents non-attenuating creep. The non-attenuating creep curve is characterised by three distinct stages: primary creep, secondary creep, and tertiary creep. During the primary creep stage, the creep rate decreases to a constant value (minimum creep rate) and remains approximately constant during the secondary creep stage. Finally, during the tertiary creep stage, the strain rate increases rapidly. If materials become susceptible to creep rupture, the consequent deformation can lead to catastrophic failure.

Three ring shear samples, denoted  $RS_i$  (where  $i = 1, 2, 3$ ), were used for the residual-state creep test. This test was carried out using two shearing procedures: the ring shear test and residual-state creep test. Firstly, samples  $RS_1$ ,  $RS_2$ , and  $RS_3$  were consolidated for 48 h under normal effective stresses of 300, 508, and 762 kPa, respectively, with the maximum effective normal stress approximately equal to the in situ overburden. Next, the samples were sheared at a controlled shear rate of 0.05 mm/min until the residual strength was obtained under a constant effective normal stress, which was applied throughout the entire creep test. This small shear rate was applied to guarantee that the pore pressure did not increase during shearing. It was assumed that all samples attained a state of residual shear strength after shearing. The basic ring shear behaviour of the shear zone soil was recorded during the first procedure. During the second procedure, samples  $RS_1$  and  $RS_2$  were reconsolidated for 24 h; next, the samples were prepared for the residual-state creep test by changing the shear mode to torque-controlled. During the residual-state creep tests, the

samples were subjected to different levels of shear stress to investigate their creep behaviour and creep threshold values. After the residual-state creep test, sample  $RS_1$  was again reconsolidated for 1, 3, and 12 days and subsequently sheared under a constant torque for the strength-regaining creep tests. A summary of the test programme is shown in Table 2. All the measurements were collected electronically, and the test data were recorded automatically by the acquisition system. The entire test programme was carried out in a constant-temperature environment to eliminate the impact of temperature variation on the deformation rates.

## Test results

### Conventional shear behaviour

Prior to the creep test, each sample was sheared by performing the standard drained strain-controlled ring shear test, thereby obtaining both the basic shear behaviour and residual shear strength. In addition, some direct shear tests were conducted using the same sample to compare with the results obtained from ring shear tests. Figure 9a shows the shear stress variation with respect to the shear displacement under various normal effective stresses. The sample under a normal effective stress ( $\sigma'_n$ ) of 762 kPa reaches peak shear strength after approximately 10 mm of shearing displacement and then exhibits a pronounced post-peak drop in shear strength; however, the other samples withstand greater shear displacements before reaching their respective peak shear strengths. With continued shear displacement after the peak shear strength, shear resistance slightly decreases to the residual shear strength.

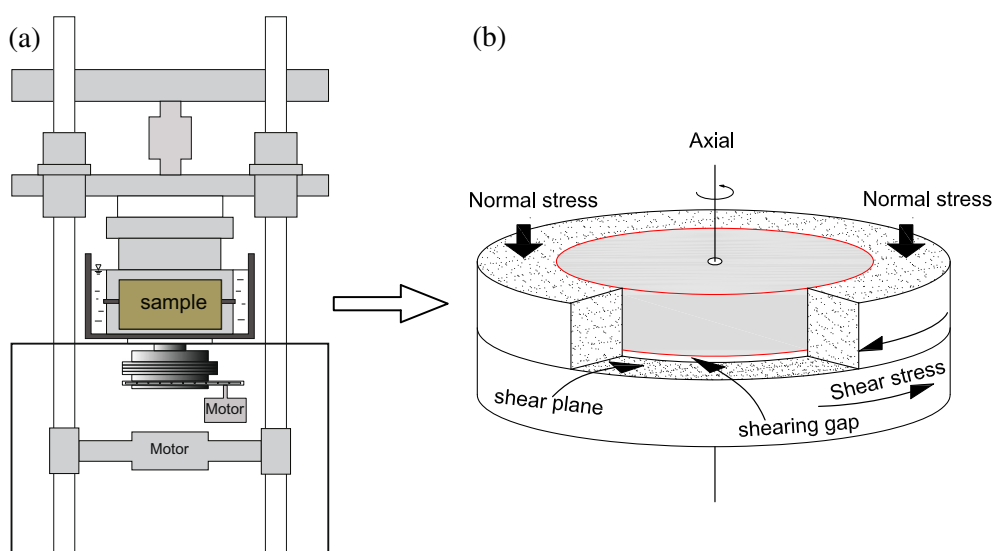


**Fig. 7** a Configuration of the ring shear apparatus. b Sketch of ring shear sample

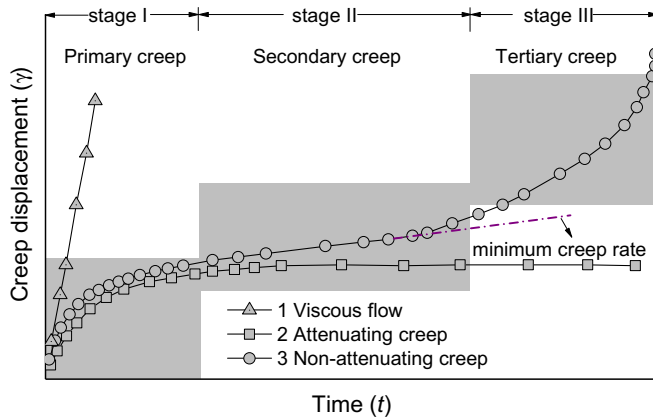


**Fig. 8** Three types of shear response to constant shear stress in a soil, together with the development of creep, characterised by three stages: primary creep, secondary creep, and tertiary creep

The shear strength envelopes obtained from the ring shear tests and direct shear tests are presented in Fig. 9b. Peak shear strength values of  $\phi'_p = 20.9^\circ$  and  $c'_p = 79.8$  kPa were obtained, similar to the results collected in the direct shear tests. In contrast, the residual strength has a non-zero cohesion component, producing a friction angle of approximately  $\phi'_r = 14.5^\circ$  and cohesion of approximately  $c'_r = 101.2$  kPa. The high cohesion and relatively low-friction angle are likely due, in part, to over-consolidation and particle bonding in the soil. In addition, the clear difference between the peak and residual strengths suggests the existence of a large domain of possible shear creep (Maio et al. 2013; Ter Stepanian 1975; Yen 1969).

#### Creep tests on pre-sheared samples in a residual state

After the normal ring shear tests, a state of residual shear strength was assumed to have been achieved in all samples. In the residual-state creep test, several stress ratios ( $R_r = \tau/\tau_r$ ) were selected to determine the applied horizontal shear stress, which was initially 90% of the residual strength, i.e.,  $R_r = 0.90$  to 1.25 and  $R_r = 0.90$  to 1.10 for samples RS<sub>1</sub> and RS<sub>2</sub>, respectively. The results obtained from the residual-state creep tests are presented in Figs. 10 and 11.

Figures 10a and 11a show that only attenuating creep occurred in the two samples under the initial shear stress ratio. An increase in the shear stress ratio to 1.03 resulted in the activation of non-attenuating creep, during which three distinct stages of creep were recorded, as shown in Figs. 10b and 11b. The corresponding relationships between the shear strain rate and creep time are presented in Figs. 10c and 11c. Sample RS<sub>1</sub> experienced 900 min of secondary creep followed by a rapid tertiary creep until failure; however, the secondary creep phase was much shorter for sample

RS<sub>2</sub>. Maio et al. (2013) evaluated the creep properties of an intact silt-clay sample, and a much longer period of creep was recorded before the sample failed in the residual-state creep test carried out using a direct shear apparatus. Here, a further increase in the shear stress ratio to 1.05 resulted in direct viscous flow with a constant shear strain rate in both samples; however, the shear strain rate in sample RS<sub>2</sub> was much higher than that in sample RS<sub>1</sub>.

#### Creep testing of samples subjected to different periods of rest

When the landslide is in a dormant phase, it is assumed that the soil in the shear zone is undergoing dormant period. To simulate this state, after the residual-state creep tests, we rested sample RS<sub>1</sub> for separate periods of 1, 3, and 12 days under an effective normal stress of 300 kPa. At the end of each rest period, creep tests were carried out under two different shear stress ratios, 1.05 and 1.10.

The variation in creep displacement with time recorded in sample RS<sub>1</sub> under the two shear stress ratios is depicted in Fig. 12. The creep rate is dramatically influenced by the rest duration. The creep rates recorded during each steady creep stage are presented in Table 3. Compared to the creep rates obtained in the 1-day rest test, the creep rates of the 3-day rest sample decreased 2000-fold under a shear stress ratio of 1.05 and 1000-fold under a shear stress ratio of 1.10. This clear decrease in creep rate indicates that the soil in the shear zone regained strength during the dormant period (Stark and Hussain 2010b), and the landslide may thus become inactive after a sufficiently long dormant phase. However, the decrease in creep rate became insignificant with a longer rest duration of 12 days.

The results of the ring shear tests conducted after 3- and 12-day rest periods are presented in Fig. 13, which shows that the regained strength led to an increase in the peak shear strength at the beginning of shearing; furthermore, the regained strength was greater after 12 days than after 3 days of rest. This result implies that the threshold of shear creep increases due to consolidation and that this increase is time-dependent. However, with increasing shear displacement, the regained strength is generally lost. Here, the shear displacement that caused the loss in regained strength was much larger than that observed in clayey soil (Stark and Hussain 2010a). One reasonable interpretation of these differences is that the clastic soil contained a significant fraction of gravel clasts (around 30 wt.%). Similar results were observed by Bhat et al. (2013b), who investigated the strength recovery ring shear test upon various landslide soils, and found that the shear displacement in which the regained strength was lost was greater in the soil with higher proportional coarse particles. With further creep displacement, as shown in Fig. 12, the creep rate may increase; this phenomenon was not observed in the present study due to the time-consuming nature of the test.

**Table 2** The programme of ring shear tests

Ring shear test name	Sample name	Normal effective stress $\sigma'_n$ (kPa)	Stress ratio ( $R_r = \tau/\tau_r$ )
Normal ring shear test	RS <sub>1</sub> , RS <sub>2</sub> , RS <sub>3</sub>	300, 508, 762	–
Residual-state creep test	RS <sub>1</sub> , RS <sub>2</sub>	300, 508	0.9, 0.95, 1.0, 1.02, 1.03, 1.05
Strength-regaining creep test	RS <sub>1</sub>	300	1.05, 1.10

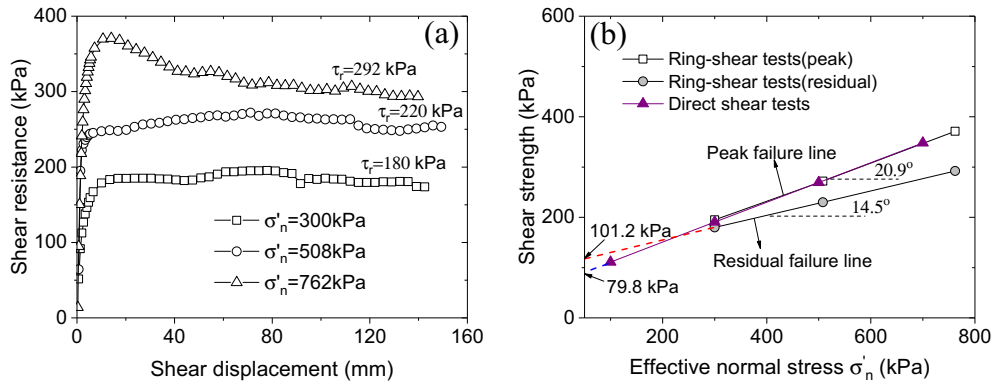


**Fig. 9** Results of ring shear tests. **a** Shear displacement against shear resistance. **b** Shear strength envelope obtained from the ring shear test and direct shear test

## Discussions

### Effects of stress ratio on creep rate

The movement patterns of the Huangtupo landslide show that it moves at different creep velocities during each active stage. Each active stage is characterised by a distinct pattern of movement, implying that the soil within the shear zone may undergo different types of creep.

The correlation between creep rates and various shear stress ratios is presented in Fig. 14; in this case, the creep rate represents the secondary creep rate recorded in the residual creep tests. As shown in Fig. 14, the creep rates slowly and linearly increase as the stress ratio increases from 0.9 to 1.0, and both samples exhibit attenuating creep. Furthermore, the creep rates nonlinearly

increase as the shear stress ratio further increases to 1.03, during which the creep is non-attenuating. As the shear stress ratio further increases to 1.05, the shear response gradually transitions from creep to viscous flow.

Analysis of Fig. 14 reveals that the dormant phase can significantly increase the creep threshold stress. Although this regained strength may be lost after a certain amount of creep displacement, a relatively low creep rate will remain until sufficient displacement occurs on the shear surface of the soil. Additionally, at each stress ratio, the creep rate recorded under an effective normal stress of 508 kPa is greater than that recorded under an effective normal stress of 300 kPa. This result implies that the shear zone material

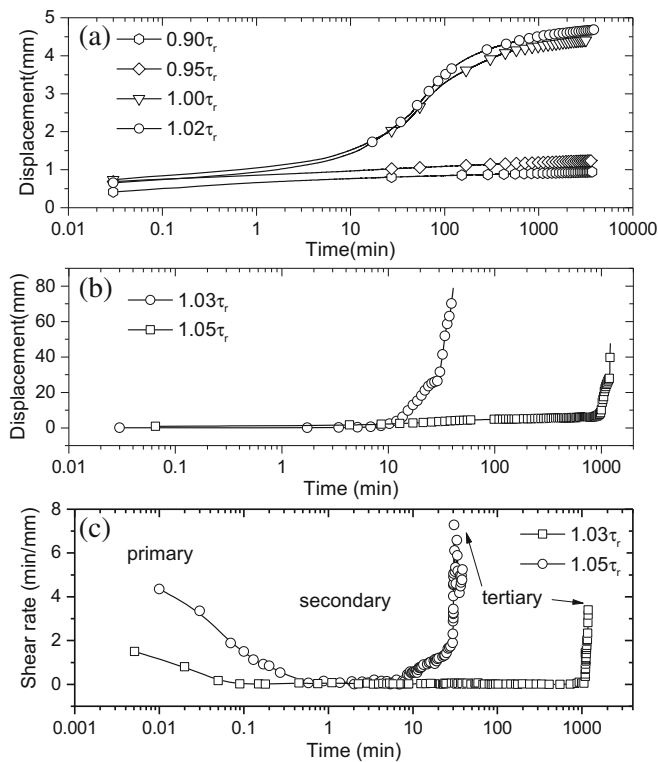


**Fig. 10** Variation in sample  $RS_1$  shear creep displacement over time under various stress ratios with **a** without failure and **b** with tertiary creep failure. **c** Creep rate variation under shear stress ratio of 1.03 and 1.05 ( $\sigma'_n = 300$  kPa)

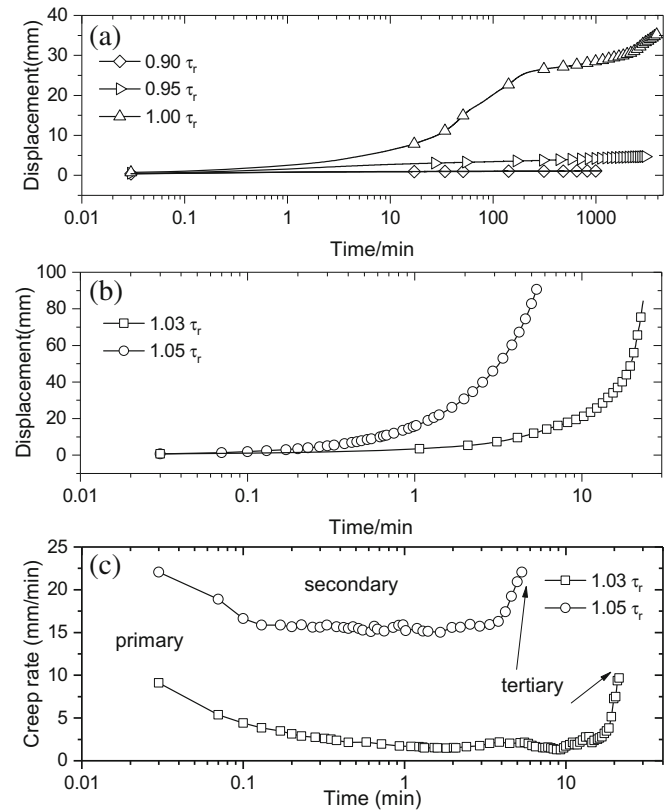


**Fig. 11** Variation in sample  $RS_2$  shear creep displacement over time under various stress ratios with **a** without failure and **b** with tertiary creep failure. **c** Creep rate variation under shear stress ratios of 1.03 and 1.05 ( $\sigma'_n = 508$  kPa)

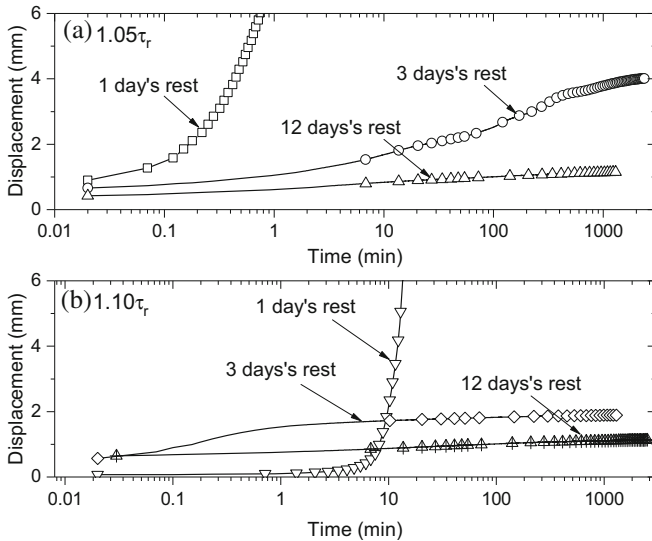


Fig. 12 Variation in creep displacement over creep time for different periods of rest

may be more likely to exhibit fluid-like behaviour under a higher normal stress level. Correspondingly, the deeper shear zone of the Huangtupo slope accounts for a greater proportion of the creep deformation than the shallow sections of the shear zone. Jian and Yang (2013), who provided additional references used in the present study, have reported similar results.

**Comparison between the long-term and the residual strength**

The long-term strength ( $\tau_r$ ) is defined as the ultimate strength observed in a creep test and corresponds to the maximum shear stress at which the creep curve decreases in constant slope and no failure is observed within the material. A shear stress above the long-term strength will drive non-attenuating creep and may eventually result in a failure. Microscopically, the long-term strength is the minimum strength under which the interparticle contacts are progressively breaking, which can lead to particle rearrangement and ultimately result in failure. This time-dependent loss in material strength is different from the loss of strength from peak to residual strength, which is the minimum strength controlled by the particle orientation after a large shearing displacement (Jiang and Wen 2015).

The correlation between long-term strength and residual strength can be obtained by isochronal curve analysis. Figure 15 presents the creep displacement recorded at different times under various shear stress ratios and normal effective stresses. The inflexion in the isochronal curve, indicated by the shaded areas in Fig. 15a, b, reveals that the long-term strength of the tested soil is nearly equivalent to its residual strength; similar results were reported by Jiang and Wen (2015), Wen and Jiang (2017) and

Table 3 Creep rate under various stress ratios and period of rest ( $\sigma'_n = 300$  kPa)

Shear stress	Shear creep rate (mm/min)		
	rest 1 day	rest 3 days	rest 12 days
$1.05\tau_r$	0.038	$1.96 \times 10^{-5}$	$1.33 \times 10^{-5}$
$1.10\tau_r$	0.088	$8.83 \times 10^{-5}$	$4.16 \times 10^{-5}$

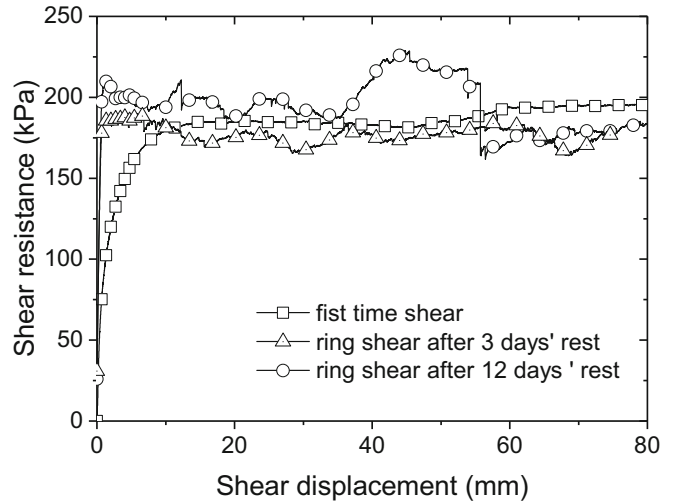


Fig. 13 Ring shear test conducted after different periods of rest ( $\sigma'_n = 300$  kPa)

Bhat et al. (2013a). However, the soil can thus undergo attenuating creep when the sustained shear stress is lower than the residual strength as well as experience non-attenuating creep and failure when the sustained shear ratio is greater than 1.0. Bhat et al. (2013a) explained that this might be due to the effects of static and dynamic friction in different creep stages. Specifically, when the stress ratio is lower than 1.0, the interparticle contacts are governed by static friction, which stabilises the sample; in contrast, when the stress ratio is greater than 1.0, the interparticle contacts are dominated by dynamic friction, which can lead to failure. However, under pre-failure conditions, the long-term strength of clastic soil is more similar to the peak strength but still higher than the residual strength (Wang et al. 2008a). Therefore, the residual strength can be considered an alternative to long-term strength for the stability analysis and prediction of slow-moving landslides with a pre-existing shear surface.

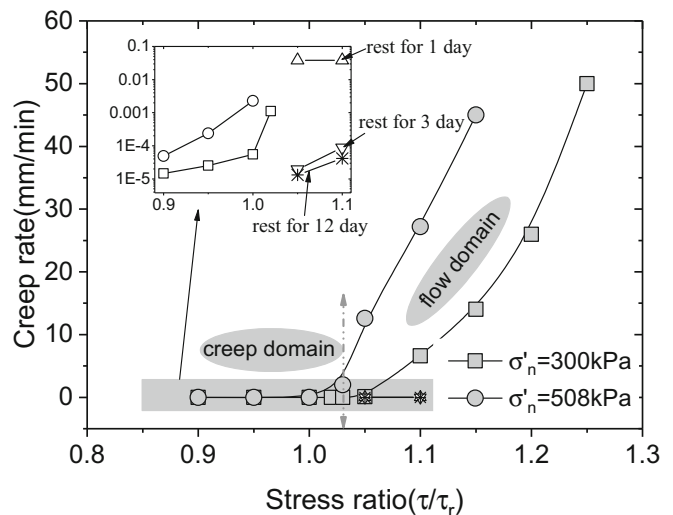
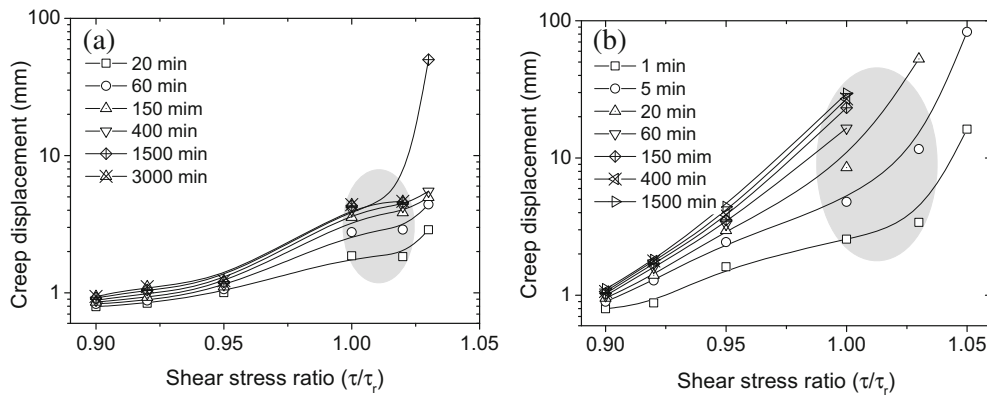


Fig. 14 Comparison of creep rate variation with increasing shear ratios under effective normal stresses of  $\sigma'_n = 300$  kPa and  $\sigma'_n = 508$  kPa





**Fig. 15** Isochronal curves under effective normal stress. **a**  $\sigma_n' = 300$  kPa. **b**  $\sigma_n' = 508$  kPa

### Conclusions

This paper discussed the creep properties of the clastic soil in the Huangtupo landslide in the TGR of China. The landslide movement patterns were first analysed from the latest monitoring results. Based on these patterns, a series of ring shear creep tests were then performed to investigate the creep properties of the clastic soil within the shear zone. The following conclusions can be drawn:

- (1) The Huangtupo landslide is moving slowly, and accumulating displacement through episodic phases of acceleration and deceleration. This movement pattern can be divided into two different processes: a creep phase, characterised by different creep rates, and a dormant phase, with different periods.
- (2) Depending on the sustained shear stress ratio, the clastic soil in the shear zone can undergo non-attenuating creep, attenuating creep, or viscous flow, while creep failure can occur only when the sustained shear stress is greater than the residual strength. In addition, a period of rest can dramatically decrease the creep rate and stabilise the soil, even if the sustained shear stress is greater than the residual strength. This finding implies that once the landslide remains dormant for a period, the stress required to remobilise the shear zone becomes higher due to strength regain. However, the regained strength can be lost with continuous shear displacement, indicating that slow-moving landslides may be reactivated with sufficient creeping movement.
- (3) For the analysed reactivated slow-moving landslide, the long-term strength of the shear zone soil is nearly equivalent to its residual strength in the residual state. However, evaluation of the residual strength is much easier and less time consuming than that of the long-term strength. For this reason, residual strength can be considered an alternative index for use in long-term stability analyses and the prediction of reactivated slow-moving landslides in the TGR.

### Acknowledgements

The authors are grateful to master student Dongsheng Xia and Dr. Liu (China University of Geoscience, Wuhan) for their help with the experiments. Finally, the authors would like to especially acknowledge the editors and reviewers of this paper, whose valuable comments led to substantial improvement.

**Funding information** Open access funding provided by University of Natural Resources and Life Sciences Vienna (BOKU). This work was funded by the National Natural Science Foundation of China (No. 41502280 and No. 41772304) and the project “GEORAMP” within the RISE programme of Horizon 2020 under grant number 645665.

**Open Access** This article is distributed under the terms of the Creative Commons Attribution 4.0 International License (<http://creativecommons.org/licenses/by/4.0/>), which permits unrestricted use, distribution, and reproduction in any medium, provided you give appropriate credit to the original author(s) and the source, provide a link to the Creative Commons license, and indicate if changes were made.

### References

- Bhat DR, Bhandary NP, Yatabe R, Tiwari RC (2011) Residual-state creep test in modified torsional ring shear machine: methods and implications. *Int J Geomate* 1(1):39–43
- Bhat DR, Bhandary NP, Yatabe R (2013a) Residual-state creep behavior of typical clayey soils. *Nat Hazards* 69(3):2161–2178
- Bhat DR, Yatabe R, Bhandary NP (2013b) Study of preexisting shear surfaces of reactivated landslides from a strength recovery perspective. *J Asian Earth Sci* 77(11):243–253
- Bishop AW, Green GE, Garga VK, Andresen A, Brown JD (1971) A new ring shear apparatus and its application to the measurement of residual strength. *Geotechnique* 21(4):273–328
- Cascini L, Fornaro G, Peduto D (2009) Analysis at medium scale of low-resolution DinSAR data in slow-moving landslide-affected areas. *ISPRS J Photogramm Remote Sens* 64(6):598–611
- Cascini L, Calvello M, Grimaldi GM (2010) Groundwater modeling for the analysis of active slow-moving landslides. *J Geotech Geoenviron Eng* 136(9):1220–1230
- Cojean R, Cai YJ (2011) Analysis and modeling of slope stability in the Three-Gorges Dam Reservoir (China)—the case of Huangtupo landslide. *J Mt Sci* 8(2):166–175
- Corominas J, Moya J, Ledesma A, Lloret A, Gili JA (2005) Prediction of ground displacements and velocities from groundwater level changes at the Vallcebre landslide (Eastern Pyrenees, Spain). *Landslides* 2(2):83–96
- Deng QL, Zhu ZY, Cui ZQ, Wang XP (2000) Mass rock creep and landsliding on the Huangtupo slope in the reservoir area of the Three Gorges Project, Yangtze river, China. *Eng Geol* 58(1):67–83
- Du J, Yin KL, Lacasse S (2013) Displacement prediction in colluvial landslides, Three Gorges Reservoir, China. *Landslides* 10(2):203–218
- González DA, Ledesma A, Corominas J (2008) The viscous component in slow-moving landslides: a practical case. In: Chen ZY et al (eds) *Landslides and engineered slopes, from the past to the future*. Xi’an, p 237–242. <https://doi.org/10.1007/s10346-012-0370-4>

- IGUS/WGL (1995) A suggested method for describing the rate of movement of a landslide. *Bull Int Assoc Eng Geol* 52:75–78
- Jian WX, Yang J (2013) Formation mechanism of No. 1 part slide of Huangtupo landslide in the Three Gorges Reservoir Area. *J China Univ Geosci (Earth Sci, in Chinese)* 38(3):625–631
- Jiang XZ, Wen BP (2015) Creep behavior of slip zone of reactivated slow-moving landslide and its characteristic strength. *Rock Soil Mech (in Chinese)* 36(2):495–501
- Jiang Y, Wang GH, Kamai T (2017) Fast shear behavior of granular materials in ring-shear tests and implications for rapid landslides. *Acta Geotech* 12(3):645–655
- Jiao YY, Song L, Tang HM, Li YA (2014) Material weakening of slip zone soils induced by water level fluctuation in the ancient landslides of Three Gorges reservoir. *Adv Mater Sci Eng* 2014:9. <https://doi.org/10.1155/2014/202340>
- Lai XL, Ye WM, Wang SM (2012) Experimental study on unsaturated creep characteristics of landslide soils. *Chin J Geotech Eng* 34(2):286–293
- Leung AK, Ng CWW (2013) Seasonal movement and groundwater flow mechanism in an unsaturated saprolitic hillslope. *Landslides* 10(4):455–467
- Li DY, Yin KL, Leo C (2010) Analysis of Baishuihe landslide influenced by the effects of reservoir water and rainfall. *Environ Earth Sci* 60(4):677–687
- Maio D, Vassallo CR, Vallario M (2013) Plastic and viscous shear displacements of a deep and very slow landslide in stiff clay formation. *Eng Geol* 162(7):53–66
- Mandl G, DeJong LNJ, Maltha A (1977) Shear zones in granular material. *Rock Mech* 9(2–3):95–144. <https://doi.org/10.1007/BF01237876>
- Mansour MF, Morgenstern NR, Martin D (2011) Expected damage from displacement of slow-moving slides. *Landslides* 8(1):117–131
- Matsuura S, Asano S, Okamoto T (2008) Relationship between rain and/or meltwater, pore-water pressure and displacement of a reactivated landslide. *Eng Geol* 101(1):49–59
- Miao HB, Wang GH, Yin KL, Kamai T, Li YY (2014) Mechanism of the slow-moving landslides in jurassic red-strata in the Three Gorges Reservoir, China. *Eng Geol* 171(3):59–69
- Okada Y, Sassa K, Fukuoka H (2004) Excess pore pressure and grain crushing of sands by means of undrained and naturally drained ring-shear tests. *Eng Geol* 75(3):325–343
- Picarella L (2007) Considerations about the mechanics of slow active landslides in clay. In: Sassa K, Fukuoka H, Wang F, Wang G (eds) *Progress in landslide science*. Springer, Berlin, p 27–45
- Prokešová R, Medved'ová A, Tábořík P, Snopková Z (2012) Towards hydrological triggering mechanisms of large deep-seated landslides. *Landslides* 10(3):239–254
- Skempton A (1985) Residual strength of clays in landslides, folded strata and the laboratory. *Geotechnique* 35(1):3–18
- Stark TD, Hussain M (2010a) Shear strength in preexisting landslides. *J Geotech Geoenviron Eng* 136(7):957–962
- Stark TD, Hussain M (2010b) Drained residual strength for landslides. *GeoFlorida2010*, GSP No. 199. ASCE, West Palm Beach, p 3217–3226
- Stark TD, Hussain M (2012) Empirical correlations: drained shear strength for slope stability analyses. *J Geotech Geoenviron Eng* 139(6):853–862
- Stark TD, Choi H, McCone S (2005) Drained shear strength parameters for analysis of landslides. *J Geotech Geoenviron Eng* 131(5):575–588
- Tang HM, Li CD, Hu XL, Su AJ, Wang LQ, Wu YP, Criss R, Xiong CR, Li YA (2015a) Evolution characteristics of the Huangtupo landslide based on in situ tunneling and monitoring. *Landslides* 12(3):511–521
- Tang HM, Li CD, Hu XL, Wang LQ, Criss R, Su AJ, Wu YP, Xiong CR (2015b) Deformation response of the Huangtupo landslide to rainfall and the changing levels of the three gorges reservoir. *Bull Eng Geol Environ* 74(3):933–942
- Ter Stepanian G (1975) Creep of a clay during shear and its rheological model. *Geotechnique* 25(2):299–320
- Tomás R, Li Z, Liu P, Singleton A, Hoey T, Cheng X (2014) Spatiotemporal characteristics of the Huangtupo landslide in the Three Gorges region (China) constrained by radar interferometry. *Geophys J Int* 197(1):213–232
- Torabi A, Braathen A, Cuisiat F, Fossen H (2007) Shear zones in porous sand: insights from ring-shear experiments and naturally deformed sandstones. *Tectonophysics* 437(1):37–50
- Van Asch TW (1984) Creep processes in landslides. *Earth Surf Process Landf* 9(6):573–583
- Van Asch TW, Malet JP (2011) Analysing the kinematic response to groundwater fluctuations of a slow-moving landslide in varved clays, using two alternatives of the equation of motion. *Supplementi di Geografia Fisica e Dinamica Quaternaria* 34:45–55
- Wang B, Zhu JB, Tang HM, Xiang W (2008a) Study on creep behavior of slip band soil of Huangtupo landslide. *J Yangtze River Sci Res Inst (in Chinese)* 25(1):49–52
- Wang FW, Zhang YM, Huo ZT, Peng XM, Araiba K, Wang GH (2008b) Movement of the Shuping landslide in the first four years after the initial impoundment of the three gorges dam reservoir, China. *Landslides* 5(3):321–329
- Wang FW, Zhang YM, Huo ZT, Peng XM, Wang SM, Yamasaki S (2008c) Mechanism for the rapid motion of the Qianjiangping landslide during reactivation by the first impoundment of the Three Gorges Dam reservoir, China. *Landslides* 5(4):379–386
- Wang S, Xiang W, Huang X, Cui DS (2012) Study of residual strength of slide zone soil under different ring-shear tests. *Rock Soil Mech (in Chinese)* 33(10):2967–2972
- Wang JE, Xiang W, Ning L (2014) Landsliding triggered by reservoir operation: a general conceptual model with a case study at three gorges reservoir. *Acta Geotech* 9(5):771–788
- Wang JE, Su AJ, Xiang W, Yeh HF, Xiong CR, Zou ZX, Zhong C, Liu QB (2016) New data and interpretations of the shallow and deep deformation of Huangtupo No. 1 riverside sliding mass during seasonal rainfall and water level fluctuation. *Landslides* 13(4):795–804
- Wen BP, Jiang XZ (2017) Effect of gravel content on creep behavior of clayey soil at residual state: implication for its role in slow-moving landslides. *Landslides* 14(2):559–576
- Yen BC (1969) Stability of slopes undergoing creep deformation. *J Soil Mech Found Eng ASCE* 95(4):1075–1096
- Zangerl C, Eberhardt E, Perzlmaier S (2010) Kinematic behaviour and velocity characteristics of a complex deep-seated crystalline rockslide system in relation to its interaction with a dam reservoir. *Eng Geol* 112(1):53–67
- Zhou CM, Shao W, Van Westen CJ (2014) Comparing two methods to estimate lateral force acting on stabilizing piles for a landslide in the Three Gorges Reservoir, China. *Eng Geol* 173(5):41–53
- Zou LC, Wang SM (2010) The research of creep model for the slide zone soil of Gushubao landslide. In: *Proceedings of the international symposium on geomechanics and geotechnics: from micro to macro*. CRC Press, Shanghai, pp 963–969

Electronic supplementary material The online version of this article (<https://doi.org/10.1007/s10346-018-1043-8>) contains supplementary material, which is available to authorized users.

#### S. Wang · J. Wang

Three Gorges Research Center for Geo-hazards,  
China University of Geosciences,  
Wu Han, 430074, People's Republic of China

#### S. Wang

e-mail: wangshun2015@gmail.com

#### S. Wang · W. Wu (✉)

Institut für Geotechnik,  
Universität für Bodenkultur Wien,  
Feistmantelstraße 4, A-1180, Vienna, Austria  
Email: wei.wu@boku.ac.at

#### Z. Yin

LUNAM University, Ecole Centrale de Nantes, GeM UMR CNRS 6183,  
Nantes, France

#### D. Cui · W. Xiang

Faculty of Engineering,  
China University of Geosciences,  
Wu Han, 430074, People's Republic of China